Albatrosses employ orientation and routing strategies similar to yacht racers

Yusuke Goto, Henri Weimerskirch, Keiichi Fukaya, Ken Yoda, Masaru Naruoka, Katsufumi Sato

PNAS RESEARCH ARTICLE | ECOLOGY
BIOPHYSICS AND COMPUTATIONAL BIOLOGY OPEN ACCESS

Albatrosses employ orientation and routing strategies similar to yacht racers

Yusuke Goto[a,1], Henri Weimerskirch[b], Keiichi Fukaya[c], Ken Yoda[a], Masaru Naruoka[d], and Katsufumi Sato[e]

Edited by Alan Hastings, University of California Davis, Davis, CA; received August 15, 2023; accepted March 15, 2024

The way goal-oriented birds adjust their travel direction and route in response to wind significantly affects their travel costs. This is expected to be particularly pronounced in pelagic seabirds, which utilize a wind-dependent flight style called dynamic soaring. Dynamic soaring seabirds in situations without a definite goal, e.g. searching for prey, are known to preferentially fly with crosswinds or quartering-tailwinds to increase the speed and search area, and reduce travel costs. However, little is known about their reaction to wind when heading to a definite goal, such as homing. Homing tracks of wandering albatrosses (*Diomedea exulans*) vary from beelines to zigzags, which are similar to those of sailboats. Here, given that both albatrosses and sailboats travel slower in headwinds and tailwinds, we tested whether the time-minimizing strategies used by yacht racers can be compared to the locomotion patterns of wandering albatrosses. We predicted that when the goal is located upwind or downwind, albatrosses should deviate their travel directions from the goal on the mesoscale and increase the number of turns on the macroscale. Both hypotheses were supported by track data from albatrosses and racing yachts in the Southern Ocean confirming that albatrosses qualitatively employ the same strategy as yacht racers. Nevertheless, albatrosses did not strictly minimize their travel time, likely making their flight robust against wind fluctuations to reduce flight costs. Our study provides empirical evidence of tacking in albatrosses and demonstrates that man-made movement strategies provide a new perspective on the laws underlying wildlife movement.

albatrosses | sailboats | wind | navigation | dynamic soaring

Significance

Albatrosses traverse substantial distances using wind energy, and their macroscale track patterns show considerable variety, ranging from beeline to zigzag. We explored the mystery of how this variability arose using mathematical models and track data from albatrosses and sailboats. We found that albatrosses employ a navigation strategy of taking zigzag routes to reach upwind or downwind goals faster (and beelines in other wind conditions) as yacht racers do. Further, the wind direction dependence of flight speed at the microscale plays a key role in albatross mesoscale and macroscale movement in the same way as in the sailboats. This study highlights the importance of determining the influence of microscale movement mechanisms on mesoscale and macroscale movement patterns to understand animal navigation.

Birds traverse great distances to reach their goals. Some species migrate across the globe from their wintering grounds to breeding grounds (1, 2), and some species undertake long-distance foraging trips during the breeding season, traveling hundreds or thousands of kilometers from their nests, and then returning to feed their chicks (3–9). These long-distance flights require significant travel costs, such as energy and time. Wind significantly impacts these cost requirements: tailwinds increase birds' speed, headwinds slow them down, and crosswinds can divert them off course (6, 7, 10, 11). Therefore, through natural selection, birds are expected to have acquired a navigational capacity that allows them to select routes that reduce travel costs under wind conditions they encounter (12–14). This macroscale route selection consists of mesoscale "orientation" processes which are decisions of travel direction, taking into account the wind and goal directions (11). Mesoscale orientation is likely determined by microscale flight dynamics, specifically, the variations in energy and time needed to travel a given distance, which depends on the travel direction relative to the wind and goal directions (15, 16). Accordingly, bird navigation in wind is hierarchically structured across three scales: micro, meso, and macro (17). To gain a deeper understanding of their navigation, we need to predict their mesoscale orientation and macroscale route selection based on microscale flight dynamics and compare these predictions with data (16). However, while bird orientation and route selection in wind conditions have been extensively studied at a macro scale, empirical research on how microscale flight dynamics shape these meso- and macroscale aspects is still limited.

Among various bird species, procellariiform seabirds (i.e., petrels, shearwaters, and albatrosses) are particularly distinctive due to their unique wind-utilizing flight style and may provide a valuable opportunity to study the implications of microscale flight dynamics on mesoscale orientation and macroscale route selection. During their breeding period, these seabirds can fly hundreds of kilometers away from their nests (3–9). During their foraging trips, birds spend only a small fraction of their flight time flapping their wings. For example, wandering albatrosses (*Diomedea exulans*), which is a study species of this study and one of the largest dynamic soaring species, only spend 1 to 15% of their flight time flapping their wings (18). This efficient travel is facilitated by a flight style known as dynamic soaring, where the birds exploit mechanical energy from the atmosphere by utilizing the wind gradient, which refers to wind speeds that increase with the altitude above the sea surface (19–21). Dynamic soaring birds exhibit a periodic flight, moving up and down within

Author contributions: Y.G., H.W., K.Y., and K.S. designed research; Y.G. performed research; Y.G. analyzed data; and Y.G., H.W., K.F., K.Y., M.N., and K.S. wrote the paper.

The authors declare no competing interest.

This article is a PNAS Direct Submission.

[1]To whom correspondence may be addressed. Email: goto.yusuke.w5@f.mail.nagoya-u.ac.jp.

This article contains supporting information online at https://www.pnas.org/lookup/suppl/doi:10.1073/pnas.2312851121/-/DCSupplemental.

Published May 21, 2024.

this wind gradient. Soaring periods are usually several seconds, 7 s (median) for Manx shearwaters (*Puffinus puffinus*) (9), and about 10 s for wandering albatrosses (22). The trajectory of a single dynamic soaring cycle appears as an elongated S-shape in the horizontal plane, with the entire trajectory being formed by repeating this pattern (22, 23). In this study, we define three spatiotemporal scales—micro, meso, and macro—for dynamic soaring birds' movement based on the number of soaring cycles. We define the movement of one soaring cycle as the microscale, which, in the case of wandering albatrosses, lasts about 10 s and covers a distance ranging from several tens to about 200 m (21, 22). The mesoscale is defined as the movement of several tens of soaring cycles, lasting several minutes, and spanning a distance of several kilometers. Last, we define the macroscale as the movement over several thousand soaring cycles, lasting several hours, and covering a distance of several hundred kilometers. Therefore, in the scales defined here, the mesoscale is approximately 10 times larger than the microscale, and the macroscale is about 100 times larger than the mesoscale.

The dynamic soaring is wind-dependent flight mechanism, which influences travel speed and energy consumption rate (24–26). Although it could affect mesoscale orientation and macroscale route selection, these aspects remain largely unexplored in spite of numerous tracking studies on procellariiform seabirds conducted over the last three decades (3, 27, 28). Previous studies have demonstrated that procellariiform seabirds tend to prefer crosswinds (9, 29–31) and quartering-tail winds (8, 24) during their foraging trips. However, it is important to note that these studies mainly focused on travel and wind directions, neglecting another crucial direction for understanding birds' navigation strategies—the direction of their goal (11).

The significance of the goal direction during the foraging trips of pelagic seabirds changes with each phase of the trip. As same as other central place foragers (32), foraging trips of pelagic seabirds are often categorized into three phases: outbound, middle, and returning (also referred to as the homing phase) (29). The factors affecting the decision-making of pelagic seabirds' travel vary between the nonhoming phases, namely the outbound and middle phases, and the homing phase. During the middle phase, the necessity to reach a specific destination is relatively weak. During the outbound phase, some seabird populations exhibited site fidelity, heading toward distinct habitats such as shelf edges, slopes, and frontal zones (33). However, the constraint to arrive at a specific location is likely weaker than in the homing phase, as birds have multiple potential foraging sites to choose from. Moreover, long-ranging seabird populations, like the wandering albatrosses incubating at Crozet Island that were studied here, show low site fidelity and lack a consistent preference for outbound direction for long trips over oceanic water (33). As a result, the diminished necessity to reach a specific site in the nonhoming phase (outbound and middle phases) makes birds to choose a travel direction that increases the distance covered per unit of travel cost. Therefore, dynamic soaring seabirds are expected to prefer crosswinds or quartering-tailwinds that enable higher travel speed and lower energy costs (24) as consistent with previous studies (8, 9, 24, 29–31, 34). In contrast, during the homing phase, the nest serves as a distinct goal. Therefore, a conflict may arise between the alignment to the goal direction and the birds' preference for crosswinds, especially when the goal is not located in the crosswind direction. Hence, it is essential to study their homing tracks under various wind and goal directions to understand how microscale locomotion dynamics (in this case, dynamic soaring) affect animal orientation and route selection—a topic that has not been extensively explored. The diverse homing tracks of wandering albatrosses may serve as a distinctive illustration of this unresolved issue. Fig. 1 illustrates the homing portion of the foraging trip of the wandering albatross, which we arbitrarily selected from previously published track data (35, 36). Their homing tracks exhibit a variety of patterns, ranging from straight lines to zigzags, similar to the tracks of sailboats (Fig. 1). This leads to a question: Is the similarity between albatrosses and sailboats trajectories merely artificial, resulting from our selective choice of tracks, or does a common underlying rule govern their patterns, possibly their response to wind?

Recent studies (21, 26) have highlighted the similarities between the mechanisms of dynamic soaring and sailing, especially regarding how wind direction impacts the travel speeds of sailboats and dynamic soaring birds, which are maximized in crosswinds and reduced in tailwinds and headwinds. The movement mechanism of a sailboat can be explained by the lift force acting on the sail and the drag force acting on the keel submerged in water (21). The lift force on the sail can be divided into components perpendicular and parallel to the direction of motion. The former is counteracted by the drag force on the keel, while the latter becomes the thrust that propels the sailboat forward. This mechanism increases the sailboat's speed in crosswinds and decreases it in headwinds and tailwinds. By plotting the sailboat's speed in polar coordinates, based on its travel direction relative to the wind direction (this plot is known as a polar diagram in sailing), the resulting shape is butterfly-like (see example ref. 37 for a sailboat polar diagram). While the movement of a sailboat can be understood through a balance of steady forces, dynamic soaring involves forces acting on birds that vary over time and involve three-dimensional movement. Hence, at first glance, this process appears quite different from sailing. However, a study pointed out similarities between dynamic soaring and sailing (21). In theoretical studies of dynamic soaring, the wind gradient above the sea is often simplified into two layers: a wind layer where constant wind blows above a certain altitude, and a boundary layer with zero wind speed below that altitude (19). In this model, dynamic soaring involves a process of moving between the wind and boundary layers. The previous study noted that the forces acting on a bird during one cycle of dynamic soaring are analogous to those on a sailboat; the forces on a bird flying in the wind layer correspond to those on a sailboat's sail, and the forces on a bird in the boundary layer correspond to those on a sailboat's keel (21). The study also argued that movement speed increases with crosswinds and decreases with tailwinds and headwinds. Although this study did not present a polar diagram for dynamic soaring, other research using numerical optimization methods theoretically determined that the polar diagram of a Unmanned Aerial Vehicle performing dynamic soaring exhibits a butterfly shape (38). Furthermore, another study reported that polar diagrams derived from albatross track data also exhibit a butterfly shape (26). These theoretical and experimental studies collectively support that the polar diagram of albatrosses exhibits a butterfly shape similar to that of sailboats.

As the speed of a sailboat depends on wind direction, yacht racers often adjust their course away from the goal if it lies leeward or windward. They alternatively switch their travel direction, known as "tacking," which results in a zigzag route on a macro scale (37, 39). This approach enables them to reach the goal more quickly. Given the wind-dependent speed similarity between dynamic soaring birds and sailboats, here we hypothesize that albatrosses adopt navigation strategies similar to yacht racers during homing to minimize travel time and energy consumption reaching their nests.

Here, we tested whether the time-minimizing strategies used by yacht racers can explain the orientation and route selection of wandering albatrosses. We predicted that when the goal is located upwind or downwind, albatrosses should i) deviate their travel directions from the goal at the mesoscale and ii) increase the number of turns at the macroscale (see *Prediction of Albatross Movement Based on Time-Minimizing Orientation Strategy by Sailors* in

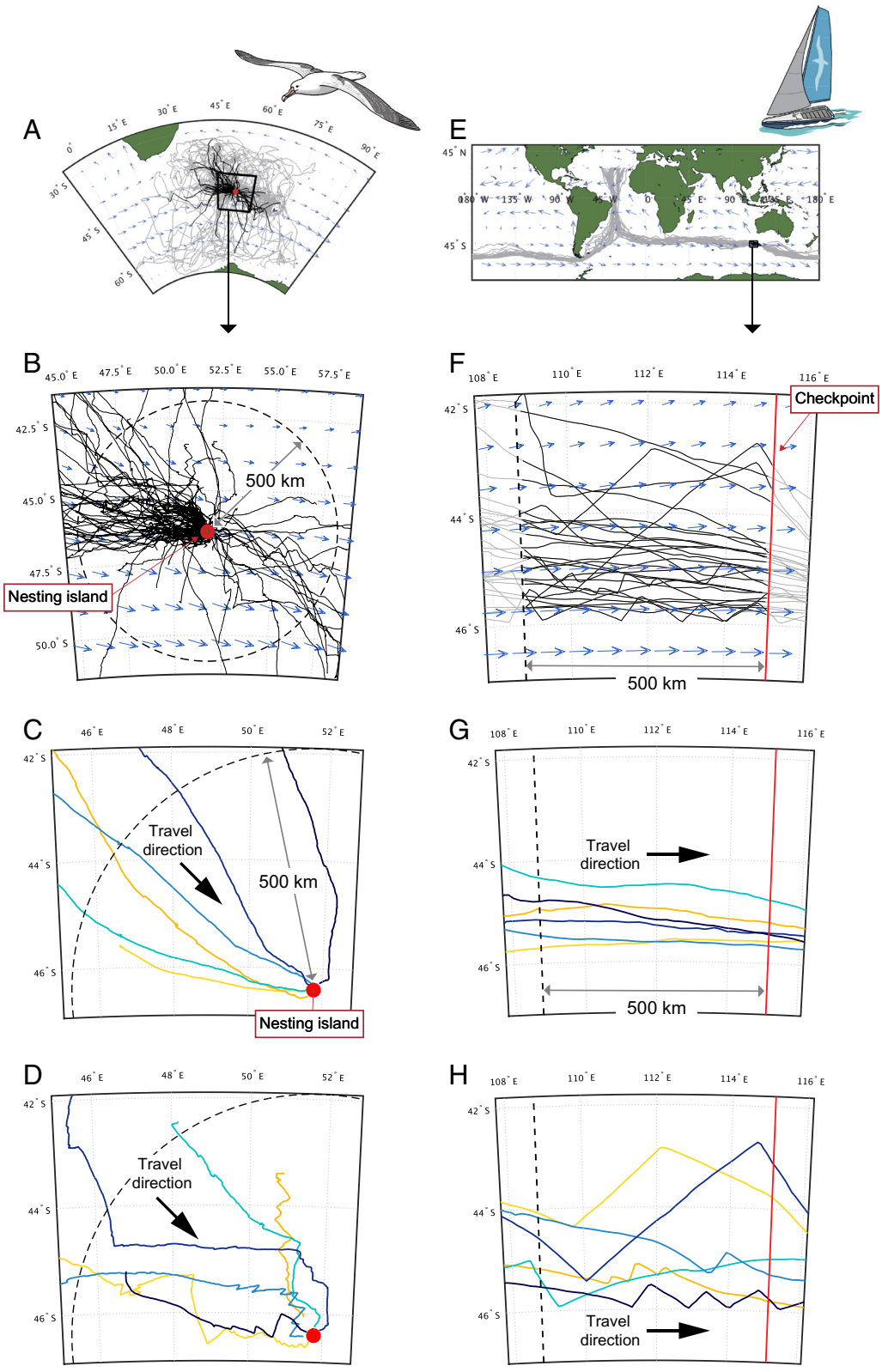

Fig. 1. Tracks of albatrosses and racing sailboats. (*A*) Foraging trips of wandering albatrosses recorded by GPS ($N = 149$). Portions of tracks in homing phase are shown in black lines and the other portions are shown in gray lines. (*B*) Homing tracks of albatrosses within 500 km from the nesting island (Possession Island). Light blue arrows in (*A* and *B*) represent average winds for January 2018 based on ERA5 ECMWF. (*C* and *D*) Homing tracks of albatrosses in straight lines (*C*) and tacking patterns (*D*) selected from trajectories shown in (*B*). Differences in color represent individuals. (*E*) Tracks of sailboats in the 2020 Vendée Globe race around the world. (*F*) Tracks (black lines) of sailboats within 500 km from the middle checkpoint (red line). Tracks in straight lines (*G*) and tacking patterns (*H*), selected from trajectories shown in (*F*). Light blue arrows in (*E* and *F*) represent average winds for December 2020 based on ERA5 ECMWF. (*G* and *H*). Differences in color represent each sailboat.

Results). We tested these predictions with tracking data from albatrosses and racing yachts in the Southern Ocean. Testing these predictions poses a challenge as it involves a detailed examination of the travel directions of homing albatrosses under various wind and goal conditions, necessitating substantial high-resolution tracking data. To address this, we utilized a comprehensive set of tracking data from their foraging trips, which comprises 149 tracks or a total of 407,659 fix data points, each recorded at a fix point every 2 min, providing a mesoscale resolution.

Results

First, we confirmed the similarities in wind-dependent travel speeds between sailboats and albatrosses (26). Thereafter, we derived predictions of albatross movement based on the time-minimizing orientation strategies used by yacht racers. Then, we tested these predictions qualitatively and quantitatively by using track data of albatrosses and sailboats.

Similarities in Wind-Dependent Travel Speeds between Sailboats and Albatrosses. We analyzed track data (1 data point every 2 min) from 149 foraging trips made by wandering albatrosses during their breeding period from Possession Island, Crozet Islands, and track data (1 data point every 30 min) from 28 yachts participating in the 2020 "Vendée Globe," a nonstop round-the-world yacht race across the Southern Ocean (Fig. 1). Both albatrosses and sailboats mainly traveled in 40 to 60°S latitudes and were constantly exposed to strong winds (average wind speed was 8.7 ± 3.4 m s^{-1} for albatross and 8.1 ± 3.0 m s^{-1} for sailboats).

We calculated the speed and direction of the albatross and sailboats by computing a vector connecting two successive data points (N = 407,659 for albatrosses and N = 102,922 for sailboats); the average distances traveled between the two observation points by the albatrosses and sailboats were 1.5 ± 0.6 km and 12.1 ± 3.4 km, respectively. Consequently, the average travel speed was 12.4 ± 5.2 m s^{-1} for albatrosses and 6.7 ± 1.9 m s^{-1} for sailboats. Their travel speed changed according to the travel direction relative to the wind direction showing butterfly-shaped polar diagrams (Fig. 2). A previous study reported that the polar diagrams of wandering albatrosses were butterfly-shaped, based on track data at around 1 h sampling intervals (26). We confirmed the butterfly-shaped polar diagrams of the sailboats and albatrosses in our data (2 min sampling intervals) by fitting nonparametric functions (*Methods*). As described below, these butterfly-shaped polar diagrams influence the movement strategies of yacht racers and are also expected to influence those of albatrosses.

Prediction of Albatross Movement Based on Time-Minimizing Orientation Strategy by Sailors. We examine situations where both sailboat racers and albatrosses have goals: Racers aim for an intermediate checkpoint, while albatrosses aim to return to their nesting island (Fig. 1). Several factors can influence their decision-making: the spatiotemporal pattern of wind conditions en route to the goal, wind-influenced speed (26), wind-dependent energy expenditure (24), and the spatial range within which they can perceive or predict wind conditions. In this study, we make two assumptions: 1) Both albatrosses and yacht racers choose their travel direction based on the local wind conditions where they are, and 2) their objective is to minimize travel time to reach their goals. The second assumption is evident in yacht racing, but we argue it is also applicable to albatrosses, for two reasons. First, by minimizing travel time, albatrosses can return to their nests sooner, thereby reducing the risk of their partners abandoning the nests, which protects the eggs or chicks (40, 41). Second, decreasing travel time leads to reduced energy expenditure, which benefits the survival and reproductive success of the albatrosses. If the dependency of energy consumption rate on the travel direction relative to the wind can be ignored, then the energy required to cover a given distance is proportionate to the elapsed travel time. Hence, elapsed time can serve as an effective proxy for energy consumption (this point will be revisited in *Discussion*).

Based on these assumptions, we derived two hypotheses from the maximum VMC (Velocity Made good on Course) strategy. This basic sailing strategy involves sailboats traveling in the direction

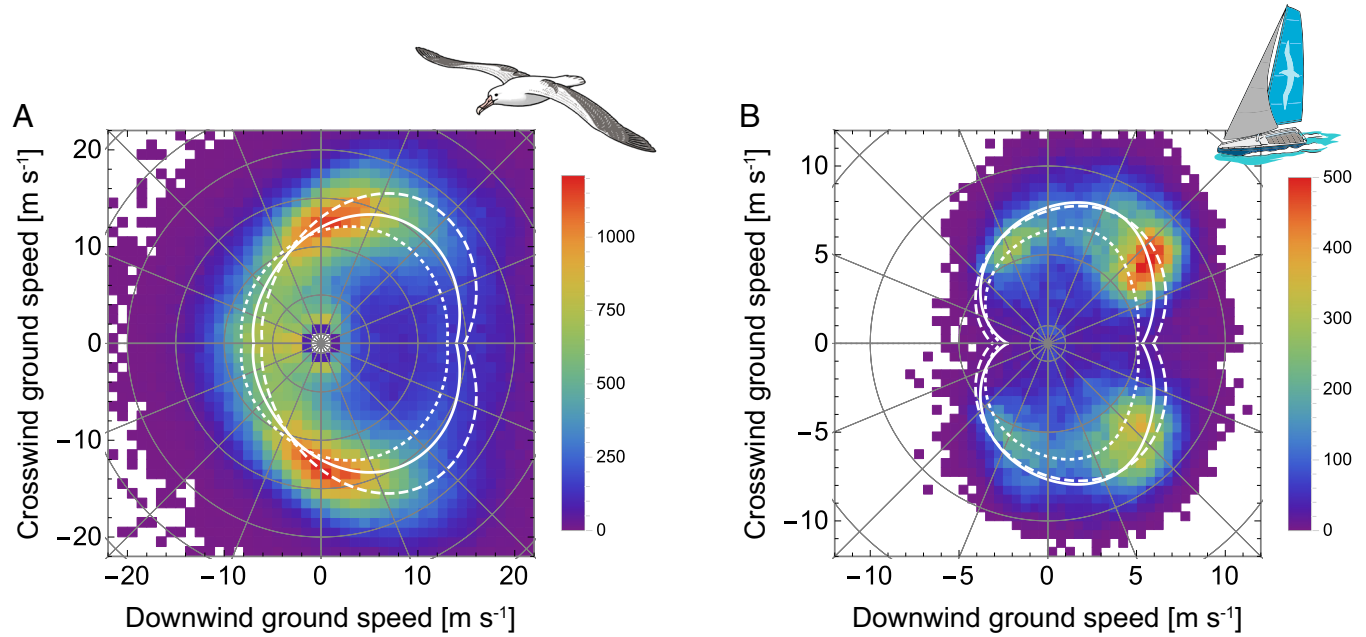

Fig. 2. Similarities in wind-dependent travel speeds between sailboats and albatrosses. Two-dimensional histogram of the ground velocity of albatrosses (*A*) and sailboats (*B*). Histograms in bins of 1 m s^{-1} for albatrosses and 0.5 m s^{-1} for sailboats. Colors represent the number of data points in each bin. The white lines indicate polar diagrams obtained by applying the generalized additive models (GAM) to the data. The solid line shows the polar diagrams with a 9 m s^{-1} wind speed, dotted lines with 6 m s^{-1} wind speed, and dashed lines with 12 m s^{-1} wind speed.

maximizing their VMC, which is defined as the component of the velocity parallel to the goal (Fig. 3*A*) (39). Under crosswind conditions, the optimal VMC direction aligns approximately with the goal direction (Fig. 3*B*). Conversely, when the goal is downwind (leeward) or upwind (windward), two high VMC directions deviating from the goal become apparent (Fig. 3*B*). This orientation also affects macroscale movement (Fig. 3*C*). Under crosswind conditions, the VMC-maximizing route tends to be a straight line. When the goal is downwind or upwind, sailors need to periodically change travel directions, a maneuver known as tacking—leading to zigzag track patterns.

To summarize our hypotheses, when the goal is located downwind or upwind, both yacht racers and albatrosses using a maximum VMC strategy are expected to deviate their travel direction from the goal (hypothesis 1) and increase the number of turns (hypothesis 2), compared to under crosswind conditions.

Qualitatively Similar Movement Patterns between Albatrosses and Sailboats. To test these hypotheses, we analyzed the tracks of sailboats and albatrosses. The Vendée Globe course begins and ends in Les Sables-d'Olonne, France, requiring a circumnavigation of the globe (Fig. 1*E*). En route, racers must cross several checkpoints, one of which is the 115°08′09″E longitude line of Cape Leeuwin (Fig. 1*F*). For the purposes of this paper, we will refer to this line as the "finish line," even though the actual race ends in Les Sables-d'Olonne. We used the tracks of sailboats within 500 km from the finish line. For albatrosses, we used the portion of their foraging trips homing to and within 500 km from the nesting island (Fig. 1*B*). Sailboats took an average of 19.3 ± 4.8 h to cover this distance, and albatrosses took an average of 20.7 ± 10.8 h (This calculation was conducted, for comparison with sailboats, using 59 trips that started their return from points beyond 500 km, out of a total of 149 trips). This duration of homing albatross is about twice the time expected based on the travel speeds depicted in Fig. 2. This is because albatrosses spend nearly half of their homing time resting on the sea surface. Specifically, they flew for an average of 11.6 ± 3.4 h and stayed on the water for 9.1 ± 3.6 h, with these sea surface stays predominantly occurring at night (*SI Appendix*, *SI Appendix01* and Fig. S1). The transition between flying and staying on the sea surface was not influenced by the goal direction to the wind (*SI Appendix*, *SI Appendix01*, *Supporting information Text 1*, and Fig. S2).

The data supported the first hypothesis. Fig. 3 *D* and *E* show histograms of the travel direction with different wind directions relative to the goal. These travel directions are every 2 min (N = 27,776) for albatrosses and every 30 min (N = 1,109) for sailboats. The peaks of the frequency distribution of travel direction for both sailboats and albatrosses deviated from the goal when it was located downwind; for albatrosses, this deviation also occurred when the goal was upwind.

The data also supported the second hypothesis (Fig. 3 *F*–*I*). We defined a macroscale turn with three parameters, i.e., rediscretizing distance s [km], the minimum segment length S [km], and the threshold for the change in travel direction at the turn η [degrees] (*Methods*). Examples of zigzag patterned tracks in downwind and upwind goals, as well as those of straight patterned tracks in crosswind goals, are shown in Fig. 3*F*. All tracks are shown in *SI Appendix*, *SI Appendix02–04*. Fig. 3 *G* and *H* illustrate the turn occurrence rate for parameters (s, S, η) = (10, 10, 30), with the goal direction to the wind direction on the x-axis and goal distance on the y-axis. Track data are displayed in light gray, with those corresponding to turns indicated by white dots encircled in red. The heat map represents the turn occurrence rate estimated from these track data (see *Methods* and, for results using different values of turn definition parameters, see *SI Appendix*, *SI Appendix01*, Table S1, and Figs. S3–S7). Fig. 3*I* represents the turn occurrence rate at distances of 100 km and 400 km from the goal. The occurrence rate of turns increased with the downwind goal for both sailboats and albatrosses and with the upwind goal for albatrosses. The turn occurrence rate varied among individuals, with some sailboats showing an increase of up to eightfold and albatrosses up to fivefold compared to the population mean (*SI Appendix*, *SI Appendix01* and Figs. S8–S12). Such individuals constituted a minority, with the majority displaying values close to the population mean. Furthermore, the extent of individual variations in turn occurrence rates (TOR) was heavily influenced by the parameters defining a turn. When both the rediscretizing distance and the minimum segment length were small, enabling the detection of finer turns, there was a high level of individual variation. When the minimum segment length was 50 km, focusing on the detection of very large-scale turns only, individual variations disappeared. In contrast, the qualitative pattern of the population's mean turn occurrence rate remained consistent regardless of the turn definition parameters (*SI Appendix*, *SI Appendix01* and Figs. S3–S7).

Differences between Movement Patterns of Albatrosses and Sailboats. While our analysis showed qualitative similarities between the movement patterns of albatrosses and yacht racers, it also implied some qualitative and quantitative differences that were further examined as follows.

(i) Albatrosses increase turns as they approach their goal. The effect of goal distance on turn occurrence rate was distinct between sailboats and albatrosses (Fig. 3*I*). In our model, parameter a determines the effect of goal distance on the turn occurrence rate. When a is positive, the turn rate decreases as a mover approaches a goal, and vice versa when a is negative. Our analysis reveals that for albatrosses, the likelihood of turning increases as they near their goal, as indicated by a negatively located posterior distribution of parameter a (*SI Appendix*, *SI Appendix01* and Table S1). Conversely, for sailboats, the inclusion of 0 in the 95% Bayesian CI for a, across all definitions of turns, suggests that we cannot assert a significant influence of goal distance on turn occurrence. This trend is evident in Fig. 3*I*, where the 75% CIs for turn occurrences at 100 km and 400 km from the goal (represented by pink shaded areas) differ for albatrosses, while those for sailboats (represented by light blue shaded areas) notably overlap.

(ii) Deviation from time minimization as primary travel cost. The observed travel direction of albatrosses slightly deviated from the time-minimizing flight directions (black arrows in Fig. 3*E*). This deviation implies that, for homing albatrosses, the time may not be the sole travel cost, a variable that animals attempt to minimize during their travel. For example, energy may be the actual travel cost. Recall that when we employed the time-minimizing hypothesis for albatrosses, we assumed their travel time to be a good proxy for energy expenditure. Thus, we have implicitly assumed that the time-minimizing strategy and energy-minimizing strategy are identical. However, given that the heart rate—an indicator of energy expenditure—in wandering albatrosses increases with headwind (24), the travel direction minimizing energy expenditure could diverge from the time-minimizing direction. This difference may explain the observed deviation.

To investigate the characteristics of the travel cost for albatross, we developed a stochastic movement model (*Methods*). Our model postulates a bird moves with a higher probability in the direction yielding a greater travel distance per cost along the goal direction. This probability is governed by the "cost function" which illustrates how the cost expenditure per time varies with the angular

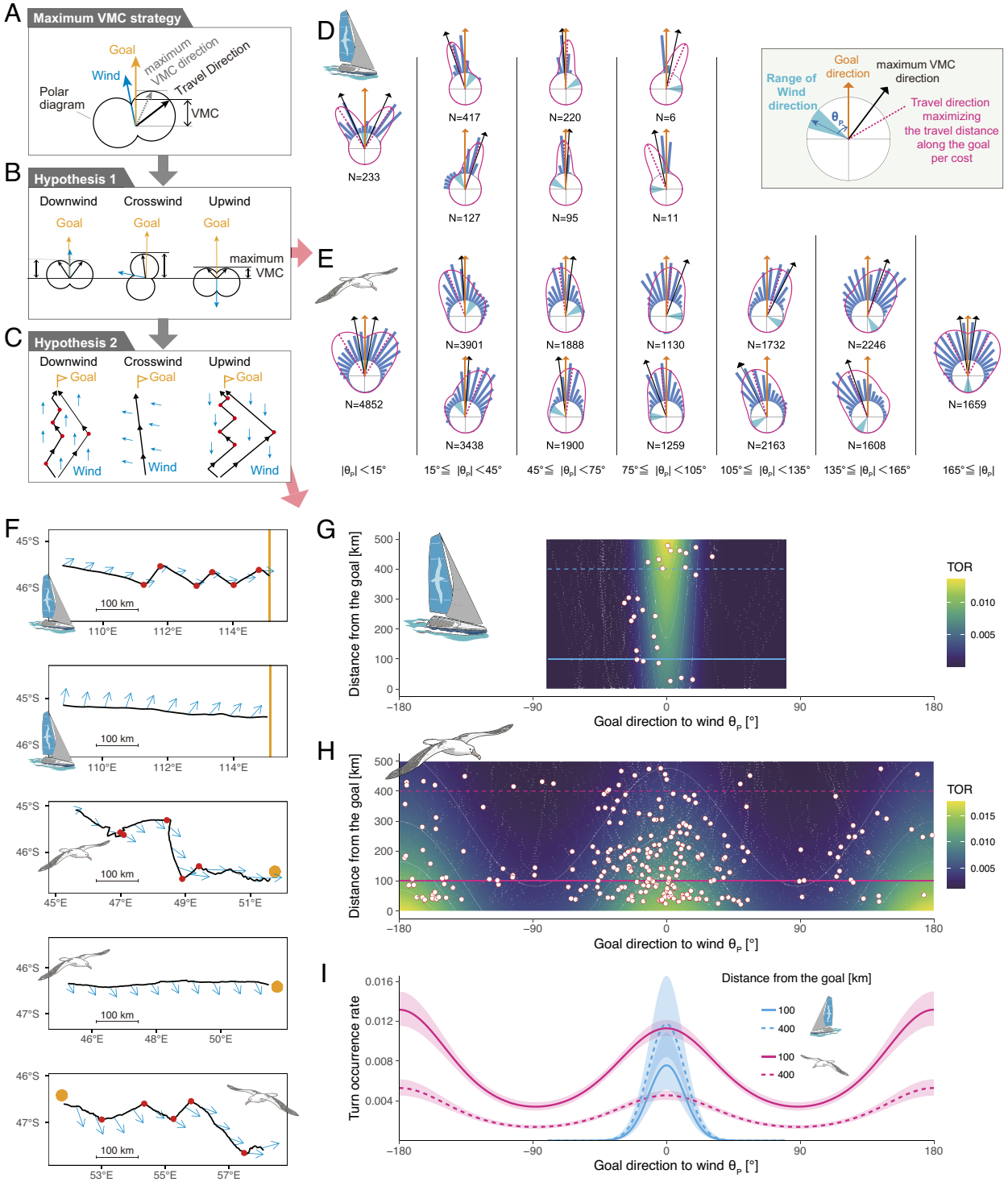

Fig. 3. Prediction of albatross movement based on time-minimizing orientation strategy by sailors, tested against track data. (*A*) Definition of VMC. (*B*) Travel directions that maximize VMC for each wind condition. Blue arrows indicate wind direction, orange arrows point to the goal direction, and black arrows indicate travel directions that maximize the VMC. (*C*) Macroscale travel patterns predicted from the maximum VMC strategy. Red points represent turning points. (*D* and *E*) Histograms of the travel direction of sailboats (*D*) and albatrosses (*E*) relative to the goal direction. Each row indicates the different wind directions relative to the goal direction. The histograms are generated from the track data in Fig. 1 (within 500 km from the finish line or nesting island). The orange arrows indicate the goal direction. The cyan fans indicate the range of wind directions relative to the goal direction. The black arrows indicate the maximum VMC directions that are calculated from polar diagram obtained from track data. Pink lines indicate the estimated distribution of track direction derived from the BIC-based selected model, and pink dashed lines indicate travel directions that maximize the travel distance along the goal per cost (see *Methods* for detail). These arrows and distributions correspond to goal directions relative to wind directions θ_p of 0°, ±30°, ±60°, ±90°, ±120°, ±150°, and 180°, with wind speeds w = 8.7 m/s for albatross and 8.9 m/s for sailboats, the average wind speeds they experienced within 500 km from the goal. (*F*) Example of tracks (black solid lines) of sailboats and albatrosses within 500 km from their goals. The orange lines show one of the middle checkpoints of the race corresponding to the longitude of Cape Leeuwin. The orange dots represent the nesting island of birds. The blue arrows represent the wind direction on the track. The red points represent the identified turning points (defined with parameters s = 10 km, S =10 km, η = 30°). When the goal was located downwind and upwind (first, third, and fifth rows), more turns occurred compared to the crosswind condition (the second and fourth rows). TOR for sailboats (*G*) and albatrosses (*H*), with on the *x*-axis and goal distance on the *y*-axis. Track data are displayed in light gray, with turns marked by white dots encircled in red. The heat map represents the TOR estimated from these track data. (*I*) TOR at distances of 100 km (solid lines) and 400 km (dashed lines) from the goal. The shaded area represents the 75% CI. Cyan lines and areas represent sailboats, and pink ones represent albatrosses.

difference between the bird's travel direction and wind direction. By testing various cost functions, we can gain insights into the characteristics of cost factors that well explain the observed travel direction. Here, we tested three cost functions that represent potential costs: constant (implied cost: time), linear (implied cost: energy), and quadratic (implied cost: unknown). See *Formulation of cost functions* in *Methods* for details. Models assuming each function were applied to the track direction data, and the best model was selected based on the Bayesian information criterion (BIC).

For albatrosses, the quadratic cost function was selected. The estimated cost function increased with headwind and tailwind (Fig. 4*A* and *SI Appendix*, *SI Appendix01* and Table S2). Utilizing the estimated cost function, the model identifies travel directions that maximize the travel distance per cost along the goal direction, depicted as pink dashed lines in Fig. 3*E*. These directions differed from those maximizing the VMC, illustrated by black arrows in the same figure. This discrepancy is especially marked in the case of downwind and upwind goals. The specific directions for θ_P values of 0°, ±30°, ±60°, ±90°, ±120°, ±150°, and 180° (where θ_P represents the angle between the goal direction and wind direction) are presented in Fig. 3*E*. For a comprehensive view across the entire range of θ_P from −180° to 180°, refer to *SI Appendix*, *SI Appendix01* and Fig. S13 *A* and *B*. These results suggest that the travel cost is not solely time or even energy and may incorporate other factors. In summary, while time serves as a reasonable proxy for travel cost given its efficacy in explaining the qualitative movement patterns of homing albatrosses, the quantitative analysis suggests the need for incorporating additional factors into the cost. Potential factors will be discussed in *Discussion*.

We conducted the same analysis on sailboats. If yacht racers were adopting a VMC maximizing strategy, a constant cost function should be selected. Contrary to our expectations, a quadratic cost function was also selected in the case of sailboats (*SI Appendix*, *SI Appendix01*, Table S3, and Figs. S13 and S14). Therefore, factors other than time may also play a role in the decisions of yacht racers. Alternatively, this result could stem from potentially inaccurate cost function estimates, given our sailboat data lacked scenarios with upwind goals. This could also be due to our simplified assumption that yacht racers base their travel direction solely on local wind conditions, neglecting the potentially more complex navigation tactics they employ. In any case, the deviation between the estimated travel direction that maximizes the travel distance per cost along the goal direction and the VMC maximizing direction for sailboats was smaller than that observed in albatrosses (*SI Appendix*, Fig. S13*B*). This suggests sailboat movement can be more effectively explained by a time-minimizing strategy compared to that of albatrosses.

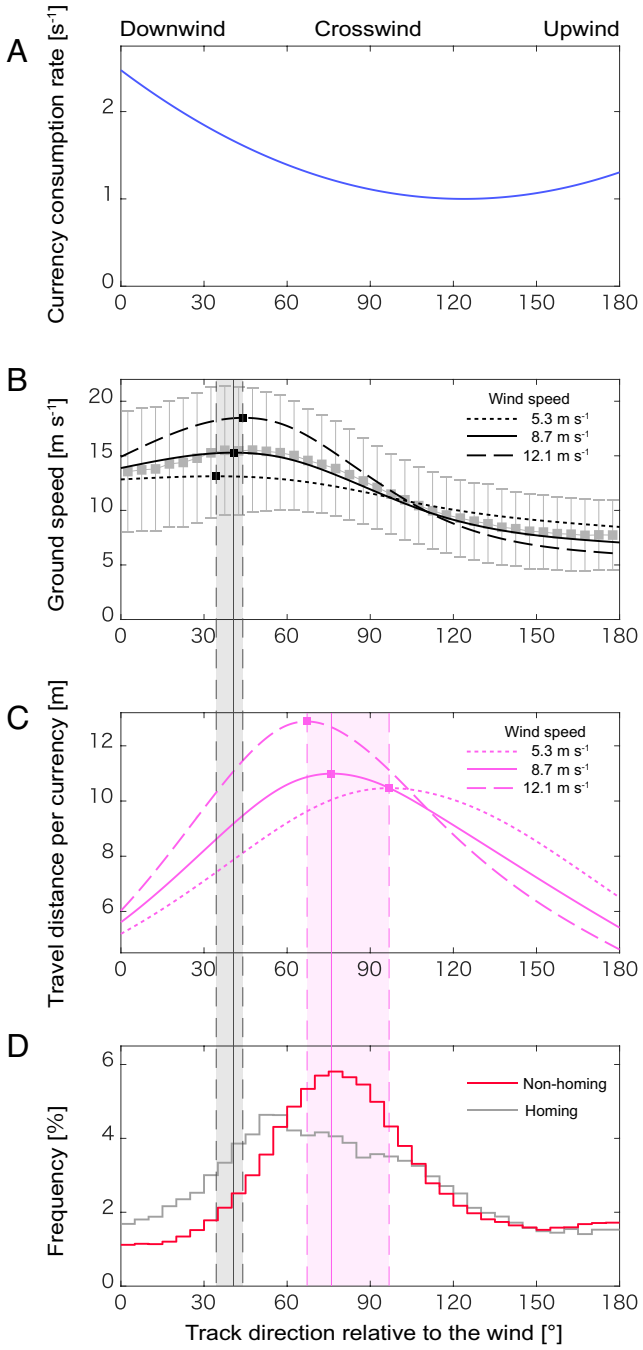

Fig. 4. Travel direction of albatrosses deviates from the speed maximizing direction. (*A*) Estimated cost consumption rate function, $C(\theta_G) = 1 + 0.314(|\theta_G| - 2.18)^2$. The horizontal axis represents the travel direction relative to the wind. (*B*) The mean and SD values of the ground speed of wandering albatrosses for all tracks are shown for each 5° of travel direction relative to the wind. The black lines correspond to the polar diagram in Fig. 2. The solid black line represents a wind speed of 8.7 m s^{-1} (the mean wind speed experienced by the albatross), the dotted line of 5.3 m s^{-1}, and the dashed line of 12.1 m s^{-1} (mean wind speed ± SD). The black squares represent the travel directions achieving the maximum ground speed for each wind speed. (*C*) The distance an albatross can travel per cost at a wind speed of 8.7 m s^{-1} (solid line), 5.3 m s^{-1} (dotted line), and 12.1 m s^{-1} (dashed line). These lines are obtained by dividing the polar diagrams in (*B*) with the cost function in (*A*). At a wind speed of 8.7 m s^{-1}, the maximum value is obtained when the travel direction of the bird to the wind is 83°. (*D*) Histogram of the travel direction relative to the wind for wandering albatrosses in the nonhoming (red, N = 374,969) and homing (right gray, N = 47,839) phases. The gray zone on panel *B*–*D* indicates the range of the travel directions achieving the maximum ground speed at wind speed from 5.3 m s^{-1} to 12.1 m s^{-1}. The pink zone on panel *C* and *D*, indicates the range of the travel directions maximizing travel distance per the cost. The peak of the frequency distribution of the travel direction to the wind is out of the gray zone, but well within the pink zone.

Discussion

This study compares the track data of wandering albatrosses and sailboats. Our results reveal that both demonstrate similar orientation and routing when heading toward their goals, albeit with some differences.

Albatrosses Show Similar Orientation and Tacking as Sailboats. Understanding how birds adjust their travel direction in response to the wind directions relative to their goal directions is fundamental to comprehending their movement strategies (11). However, the interrelation between travel direction, wind direction, and goal direction has rarely been explored in dynamic soaring birds. Although previous studies have reported that dynamic soaring birds prefer crosswinds (9, 29–31) and quartering-tailwinds (8, 24), these studies primarily examined the relationship between only

the wind direction and the bird's travel direction. Our study found that, similar to sailboat racers, albatrosses flexibly adjust their travel direction based on the goal direction relative to the wind. They deviated from leeward and windward goals in mesoscale movements (1 to 2 km) and switched direction more frequently when the goal is upwind or downwind in macroscale movements, with some tracks showing clear zigzag patterns (Fig. 3*F* and *SI Appendix*, *SI Appendix02* and *03*). It should be noted that this macroscale zigzag completely differs from the well-known microscale S-shape track pattern of one dynamic soaring cycle (23, 42, 43), which some studies have referred to as the repetition of this S-shaped pattern as zigzag (44).

This study provides empirical evidence that albatrosses adjust their direction of movement in response to wind direction similar to sailboat racers. Two studies (34, 43) have reported that tracks of albatross proceeding upwind exhibit zigzags at 100 m to 1 km scales, and this phenomenon was discussed using yacht tacking as an analogy (26, 43). However, these discussions were relied on data visually selected from the complete datasets, totaling approximately 20 km. Moreover, a recent study has reported "zigzag flights" during the foraging trips of Bulwer's petrels (30). These zigzag patterns, observable in the nonhoming phase, involve sharp turns resulting in direction changes of up to 180 degrees. This zigzagging was concluded to be an efficient prey search strategy, as it increases both the travel distance per unit energy expended and the olfactory scanned area for detecting foraging opportunities (30). Thus, this zigzag flight found in Bulwer's petrels (*Bulweria bulwerii*) stems solely from a preference for crosswinds and is different from tacking, which arises from a tension between the preference for crosswinds and the necessity to move toward a specific goal. To confirm tacking in birds, merely identifying zigzag patterns in their flight tracks is not enough; it is crucial to quantify how the occurrence of zigzag patterns changes depending on wind and goal directions during the homing phase (i.e., whether the wind is blowing headwind, downwind, or crosswind to the goal). By examining this point, we provided experimental evidence of tacking behavior in wildlife.

Albatrosses increase turns as they approach the goal. We found an increase in the turn occurrence rate as albatrosses neared their goals, a trend absent in sailboats. This could be attributed to the differences in their navigation goals: Sailboats aimed to pass the middle check point line, allowing some flexibility, while albatrosses targeted a specific point. In a study investigated the migration of loggerhead turtles (*Caretta caretta*) in response to ocean currents, it was reported that the turtles initially moved in an approximate direction toward their goal and later changed their travel direction to offset deviations in the later stage of migration (45). The increased rate of turns as albatrosses approach their goal suggests that they may have adopted a similar strategy, initially flying broadly toward their nests and then increasing the occurrence of turns to fine-tune their track as they near their final destination.

Albatrosses do not maximize their speed. Our findings suggest that the travel cost for albatrosses during their homing phase cannot be attributed solely to time or energy. This challenges the prevailing understanding that dynamic soaring birds, such as albatrosses, favor crosswinds or quartering-tailwinds to optimize their travel speed (8, 24). The prey of albatrosses is widely and patchily distributed over the sea. Therefore, in populations with low foraging site fidelity, during their foraging trips (excluding the homing phase), the priority should be to maximize the encounter rate with prey. This implies that albatrosses are expected to choose a direction that optimizes travel distance per unit cost during the nonhoming phase. A previous study demonstrated that wandering albatrosses prefer the speed-maximizing direction during foraging trips, suggesting that their travel cost is time (or energy) (24). Comparable findings have been reported for Desertas petrels (*Pterodroma deserta*), another dynamic soaring species (8).

However, these studies analyzed the entire trip and thus did not differentiate between the nonhoming and homing phases. Our results suggested that time was not the sole cost during the "homing" phase for wandering albatrosses. To reconcile our findings with those of previous studies, we propose two possible hypotheses. The first hypothesis is that time is the travel cost during the nonhoming phase (based on previous studies) but not during the homing phase (based on our results). The second hypothesis is that the travel cost cannot be attributed solely to time even during the nonhoming phase. Although the second hypothesis contradicts the results of previous studies, it is worth noting that the tracking data used in those studies had a coarse temporal resolution of 1- to 2-h sampling intervals (8, 24). This could potentially obscure the detection of mesoscale movement patterns. We calculated the travel direction of albatrosses during the nonhoming phase from our data, recorded at 2-min intervals (Fig. 4*D*). Unlike coarser resolution tracks used in previous studies, our data indicated that the peak of travel direction distribution deviated from the speed-maximizing direction (black lines in Fig. 4*D*). However, it closely aligned with the direction that maximizes travel distance per the cost which was estimated from the homing segments of the tracks (pink lines in Fig. 4*D*). Therefore, these results support the second hypothesis. Our data suggest that albatrosses incur the same cost during both the nonhoming and homing phases, implying the possible contribution of factors other than time or energy to the travel cost throughout their foraging trip.

Speed or Robustness: Which Is Prioritized for the Dynamic Soaring Birds in Fluctuating Winds? What then constitutes the additional cost? While our current results cannot identify it definitively, one potential contributor could be the risk of costly flapping flights due to the unpredictability of wind conditions. Soaring birds are spared from flapping flight by exploiting the energy from wind. However, dynamic and unpredictable wind conditions may necessitate birds to engage in costly flapping flights. Hence, for soaring flight, not only efficiency (i.e., time or energy minimization in predictable wind) but also the robustness to stochastic changes in the winds should be key factors, whereby birds try to minimize the duration of flapping flight. This is particularly important for larger species such as the wandering albatross, which rarely uses flapping flight (18).

This risk-aversion strategy is already known in thermal soaring birds (46–48). Thermal soaring is a flight style in which birds repeatedly ascend with updrafts (convection currents) and then glide. If birds are aware of the distance and updraft speed of successive thermals, the theory suggests an "optimal speed" to maximize their horizontal travel speed (49, 50). However, in practice, larger bird species tend to employ a slower airspeed than the optimal speed (46). The slower airspeed allows them to cover longer distances with a smaller loss in altitude (in contrast to that, optimal speed enables longer distance with shorter time). This tactic mitigates the risk of the birds losing height before finding the next stochastically distributed thermal, thus avoiding the risk of being forced to conduct costly flapping flights (46).

Our results may suggest that dynamic soaring species may also employ a risk-aversion strategy. The theory of dynamic soaring often assumes wind gradients to be temporally invariant (21, 51, 52). However, real wind gradients are turbulent and exhibit spatiotemporal fluctuations at microscale and mesoscale (53). Moreover, dynamic soaring birds fly near the sea surface, where the wind gradient becomes quite complicated due to the interplay between wind

and waves (54). This uncertainty in wind conditions at microscale and/or mesoscale may drive albatrosses to prioritize the efficiency of harvesting mechanical energy from wind gradients over flight speed. In dynamic soaring, a trade-off exists between speed and the mechanical energy harvesting from the wind (9): The equation of motion shows that the kinematic energy flow from wind gradient to the bird increases when the bird aligns its flight direction upwind during ascent and downwind during descent (9, 20, 21). Therefore, compared to a strategy that prioritizes energy harvesting, a strategy that maximizes speed may be more prone to unexpected wind changes and carry a higher risk exhausting mechanical energy needed to stay aloft, potentially leading to costly flapping flights. To avoid this risk, wandering albatrosses may favor travel directions that prioritize energy-harvesting efficiency, even if it results in slower speeds. Future work could focus on testing whether dynamic soaring birds prioritize energy-harvesting efficiency over travel speed. This would be an intriguing prospect, but it is technically challenging due to the need for the detailed wind information and simultaneous recording of detailed tracking, body posture, and air speed of the bird at high resolution.

Navigation Strategies of Yacht Racers Provide a New Perspective on Seabird Navigation. Pelagic seabirds are unique in the animal kingdom, with their extensive track data offering invaluable opportunities to explore wildlife movement in response to the surrounding environment (28, 55–57). This study demonstrates that insights from sailboat racers and engineers can aid in decoding these extensive data to reveal fundamental patterns of pelagic seabird locomotion, laying the groundwork for further exploration. While our study simplistically assumed that albatrosses choose their travel direction based solely on local wind, birds may perceive or predict larger-scale wind conditions and adjust their travel direction accordingly (8, 24, 30). This consideration is particularly important when birds undertake long-distance travel, as the optimal route can differ between static wind conditions and those that change spatiotemporally at macroscale (17). The homing albatrosses we studied experienced changes in wind direction exceeding 30 degrees in 10% of cases after 1 h, 25% after 2 h, and 40% after 3 h, and changes in wind speed of more than 3 m/s in 5% of cases after 3 h (*SI Appendix*, *SI Appendix01*, *Supporting Information Text 2*, and Fig. S15). Therefore, although wind changes were not significantly large in our study, albatrosses indeed experience wind changes during their travel. How these birds adjust their movement in response to macroscale wind changes warrants further exploration in future research. Autonomous sailing algorithms could be useful to further investigate these intricate movement strategies (58, 59). Such algorithms determine the optimal travel direction by incorporating global-scale wind predictions (58, 59). Applying these man-made movement strategies as testable hypotheses to pelagic seabirds' movement could help uncover the travel costs and cognitive capabilities of these species, thereby offering interesting directions for future investigation.

Methods

Track Data. We used the track data of wandering albatrosses from 2003 to 2005 and 2016 to 2019 collected in previous studies (35, 36, 60) (Fig. 1 *A*–*D*). All data were obtained from breeding individuals on Possession Island (46°25′S, 51°45′E). Loggers were attached on the back feathers with TESA tape during a shift change with their partner. Loggers were retrieved when they returned to the nest after foraging. Loggers weighed 60 to 75 g in the 2016 to 2019 studies (36, 60); in the 2003 to 2005 study (35), in addition to the 45 g GPS logger, birds swallowed a 20 g stomach temperature tablet that transmitted stomach temperature to a recorder, and the 25 g recorder was attached to their backs, for a total device mass of 90 g. In all studies, the total mass of the equipment was less than 3% of the birds' mass. See each study for more detailed information (35, 36, 60).

Portions of tracks within 20 km of the Island were excluded from the analysis to avoid the influence of land. Trips of incomplete recordings that stopped before the nest was reached were excluded from the analysis. In total, we obtained data for 149 foraging trips. An iterative forward/backward averaging filter was applied to each track to exclude unrealistic points with speeds of more than 100 km h^{-1}. Furthermore, since sampling intervals differed among the data (10 s to 2 min), the data were resampled every 2 min. For each track, we defined the homing start points employing a backward path analysis (61, 62) (*SI Appendix*, *SI Appendix01*, *Supporting Information Text 3*, and Fig. S16).

Additionally, data from the Vendée Globe, a long-distance yacht race held in 2020, were used for sailboats (Fig. 1 *E*–*H*). Of the participating boats, we used data from 28 boats that passed through the middle checkpoint (longitude 115°08′09″E line). For the analysis, we used the route below a latitude of 30 degrees north. The positions of all the boats were recorded every 30 min.

Calculation of Ground Velocity Vector, Wind Vector, and Goal Direction. For each data point, we calculated (i) the ground velocity vector (travel direction and speed relative to the ground) and (ii) wind direction and wind speed. In addition, for data points in the homing phase and within 500 km of the goal, we also calculated (iii) the direction of the goal as follows.

(i) Ground velocity (ground speed and travel direction). The ground velocity was calculated for each position by dividing the vector connecting two consecutive data points by the elapsed time. Since there were some instances of recording deficit, the ground velocity was not calculated for data points corresponding to these deficits; i.e., the ground velocity vectors were calculated only when there was a pre-resampling data point within 2 min before and after the two consecutive post-resampling data points. The track data included data when the albatross was staying at the sea surface. The histogram of albatross travel speeds has two distinct peaks: one at 0 m/s, indicating periods of stay on the water, and another at a higher speed indicating flight (*SI Appendix*, *SI Appendix01* and Fig. S17). Based on this figure, we visually defined a speed threshold, classifying data points with speeds less than 2 m/s as stay on the sea surface, thus excluding them from the analysis.

(ii) Wind direction and speed. For the wind direction and speed data, we used ERA5 ECMWF, hourly on a 0.25° grid (https://cds.climate.copernicus.eu/cdsapp#!/dataset/reanalysis-era5-single-levels). This corresponds to an approximate resolution of 15 to 30 km at the latitudes of tracks used in this study. We selected winds at 10 m above the surface of the Earth, as this height closely aligns with the mean (8 m) flight heights observed in wandering albatrosses (42). The wind direction is not expected to change drastically at this height. While the average wind speed experienced by birds should be affected by the wind gradient, making it weaker than the ECMWF wind speed data (26), the primary interest of this study is the wind speed index rather than specific wind values, for which the ECMWF data is aptly suited. For each track data point, the estimates of wind direction and speed predictions at the closest point in time and distance were used.

(iii) Goal direction. The direction of the goal from the bird or sailboat was calculated for each data point for data within 500 km from the goal in the homing part of albatrosses and within 500 km from the finish line of the sailboat. For the albatrosses, the goal direction was calculated from GPS observation points, setting Possession Island as the goal, and for the sailboats, the goal direction was set to due east.

Identification of Polar Diagram Using GAM. Based on the ground velocity vector and the wind vector obtained in the previous section, the polar diagrams of the albatrosses and sailboats were determined using a generalized additive model (GAM), a nonparametric smoother method (63). The ground speed (V) was used as the response variable, and the absolute value of the direction of movement relative to the wind (θ_G: difference between the travel direction and the wind direction, see *SI Appendix*, *SI Appendix01* and Fig. S18) and the wind speed (w) were the explanatory variables. The calculations were performed in R v3.6.3 with the "gam" function of the "mgcv" package. We employed the "te()" function setting the tensor product smooths for the model formula (63). From these, the ground speed was obtained as a function of the wind speed and the direction of movement relative to the wind direction, i.e., $V(\theta_G, w)$, and the polar diagram was obtained by displaying this function in polar coordinates.

Testing the Effect of Goal Direction to Wind on Turn Occurrence Rate. Here, we test the effect of the goal direction to the wind on the turn occurrence in the macroscale movement of albatrosses and sailboats. We analyzed the portions of sailboat and homing albatross tracks within from 500 km away from the goal. For albatrosses, to exclude exceptionally short homing tracks, those with a starting point located less than 100 km from the goal were omitted from the analysis. Consequently, 107 albatross tracks were analyzed.

(i) Definition of a turn. We analyzed time-series data of travel directions for albatrosses and sailboats to identify turns. We rediscretized each track to consist of steps with a constant distance of s km. In a straight track, the travel direction remains constant over time. However, a track with turns consists of multiple distinct segments, each characterized by a different constant direction (*SI Appendix*, *SI Appendix01* and Fig. S19). A turn is defined when consecutive segments exceed a threshold length, S km, and the angular change between these segments surpasses a threshold, η degrees. The turn detection process is detailed in *SI Appendix*, *SI Appendix01*, *Supporting Information Text 4*, and Fig. S20.

In this definition, three parameters are involved: the rediscretizing distance s [km], the minimum segment length S [km], and the threshold for the change in travel direction at the turn η [degrees]. Additionally, for albatrosses, there are two definitions for the turns to be analyzed: whether to exclude turns involving water landings or not. To investigate the robustness of our results to the values of these parameters defining turns, we employed several combinations of values. Specifically, we used $s = 1$, 10 for albatrosses, and 10 for sailboats, $S = 5$, 10 for $s = 1$ and 10, 50 for $s = 10$, and $\eta = 30$, 45. Therefore, for albatrosses, we defined turns according to the above procedure with 16 different combinations of parameters, and for sailboats, with 4 different combinations. Among them, we presented rediscretized tracks illustrating defined turns for albatrosses with parameters $s = 10$, $S = 10$, and $\eta = 30$ in *SI Appendix*, *SI Appendix02*; $s = 1$, $S = 10$, and $\eta = 30$ in *SI Appendix*, *SI Appendix03*; and for sailboats with $s = 10$, $S = 10$, and $\eta = 30$ in *SI Appendix*, *SI Appendix04*.

For each rediscretized data point of individual i, we defined turn occurrence $\chi_{i,k}$ (assigned as 1 if a turn occurs and 0 otherwise) following the above steps, and also calculated both the goal direction to the wind ($\theta_{P,i,k}$ [degrees]) and the distance to the goal ($D_{i,k}$ [km]), where k (=1,...,N_i) represents the index of rediscretized data that begins at the homing start point (or at the point where the homing track first enters within 500 km if homing starts more than 500 km away). The total number of data points for individual i is represented by N_i.

(ii) Effect of goal direction to the wind on turn occurrence. Using the dataset defined above, we evaluated the effect of goal direction to wind and distance from the goal on the occurrence of turns. We assumed that the probability of a turn occurrence probability rate at position k for individual i, denoted as $P(\chi_{i,k})$, is given as:

$$\begin{aligned} P\left(\chi_{i,k}=1\right) &= \lambda_{i,k}s, \\ P\left(\chi_{i,k}=0\right) &= (1-\lambda_{i,k})s, \end{aligned}$$

where s is the resampling scale used to define turns. For albatrosses, the $\lambda_{i,k}$ is given as:

$$\lambda_{i,k} = \exp\left[r_0 + r_i + aD_{i,k}/100 + b_1\cos\left(\theta_{P,i,k}\right) + b_2\cos\left(2\theta_{P,i,k}\right)\right],$$

and for sailboats,

$$\lambda_{i,k} = \exp\left[r_0 + r_i + aD_{i,k}/100 + b_1\cos\left(\theta_{P,i,k}\right)\right].$$

The coefficient a represents the effect of the goal distance on the turn occurrence rate. When a is positive, the turn occurrence rate increases as the mover approaches the goal, and vice versa when a is negative. The coefficients b_1 and b_2 represent the influence of wind direction on the turn occurrence rate. The term $b_1\cos\left(\theta_{P,i,k}\right)$ peaks at the leeward goal when b_1 is positive, and at the windward goal when negative. The term $b_2\cos\left(2\theta_{P,i,k}\right)$ has peaks at both the leeward and windward goals when b_2 is positive, and peaks at crosswinds when negative. Therefore, the term $b_2\cos\left(2\theta_{P,i,k}\right)$ is essential to test our hypothesis that the turn occurrence rate increases in both cases where the goal is located leeward or windward. However, we omitted this term from the sailboat model for simplicity, as our sailboat dataset lacked conditions where the goal is located upwind. The random effect r_i represents the deviation of individual i's turn occurrence rate from that of population mean. Individual i is e^{r_i} times more likely to turn compared to the population mean turn occurrence rate. The r_i follows a normal distribution with mean 0 and SD σ_r,

$$r_i \sim N\left(0, \sigma_r\right).$$

Models were fitted with the rstan package, running 4 chains of 55,000 Markov chain Monte Carlo iterations, with the first 5,000 steps as the burn-in period. For each parameter, the median and 95% credible interval (CI) of posterior distributions were reported (*SI Appendix*, Table S1). Using the estimated posterior distributions of parameters (r_0, a, b_1, b_2), we calculated the median, 75% CI, and 95% CI of the population mean turn occurrence rate $\lambda(\theta_P, D) = \exp\left[r_0 + aD/100 + b_1\cos\left(\theta_P\right) + b_2\cos\left(2\theta_P\right)\right]$ for albatrosses, and $\lambda(\theta_P, D) = \exp\left[r_0 + aD/100 + b_1\cos\left(\theta_P\right)\right]$ for sailboats, with θ_P ranging from $-180°$ to 180° and D from 0 to 500. We plotted the median of $\lambda(\theta_P, D)$ and, for $D = 100$ and 400, plotted the median and CIs of $\lambda(\theta_P, D)$, see Fig. 3 *H* and *I* and *SI Appendix*, *SI Appendix01* and Figs. S3–S7. We also quantified and visualized the variation in TOR among individuals. For each track, we plotted the median of e^{r_i} with respect to the posterior distribution of r_i, against the angular mean of $\theta_{P,i,k}$ with respect to the index k (*SI Appendix*, Figs. S8–S12).

Model to Estimate Travel Cost from Track Data. We have developed a stochastic movement model to determine the "travel cost" that best explains albatross movement data. Our model considers bird flight in a two-dimensional space. Here, we denote wind speed as w, the angular difference between the bird's ground velocity and the wind velocity as θ_G, and the angular difference between the goal direction and the wind velocity as θ_P (*SI Appendix*, Fig. S18). Our model is based on the premise that a bird is more likely to move in a direction that closely aligns with maximizing the "distance traveled in the goal direction per unit of cost spent." This likelihood is determined by a cost function that quantifies the rate of cost expenditure depending on θ_G. The aim of our model is to estimate the form of this cost function using empirical data, thereby gaining insights into the nature of the travel cost for albatrosses. First, we present the model formulation to describe the bird's travel direction (Step 1), then we discuss potential options for the cost function (Step 2), and finally, we estimate the cost function by fitting the model to the data (Step 3).

[Step 1] formulation of the model. We define the cost function $C\left(\theta_G\right)$ as the cost consumed per unit time during a bird's flight in the direction of θ_G. We assume the cost function only depends on θ_G for simplicity. The specific form of the cost function will be discussed in subsequent steps.

We then formulate the distance traveled in the goal direction per unit of cost spent using the cost function. For this purpose, we used the concept of Isotropic Energy Polygons (IEPs) proposed in a previous study (16). IEPs graphically represent the distance an animal can travel per unit energy spent. In our case, i.e., two-dimensional bird flight, the IEP is a polar plot of $L_E\left(\theta_G, w\right)$ with respect to θ_G, where the function $L_E\left(\theta_G, w\right)$ represents the distance covered by a bird per unit energy spent under given travel direction θ_G and wind speed w. Following this idea of IEPs, we propose Isotropic Cost Polygons (ICPs), a generalized version of IEPs that is characterized by the distance a bird can travel per unit of "cost" spent. Hence, an ICP is a polar plot of $L_C\left(\theta_G, w\right)$ which represents the distance covered per unit cost. Using ICPs (*SI Appendix*, Fig. S18), the distance traveled in the goal direction per unit of cost spent, denoted as $F\left(\theta_G \mid \theta_p, w\right)$, is given by

$$\begin{aligned} F\left(\theta_G|\theta_P, w\right) &= \vec{\boldsymbol{L}}_c \cdot \vec{\boldsymbol{n}}_P \\ &= L_C\left(\theta_G, w\right)\left(\cos\theta_G\cos\theta_P + \sin\theta_G\sin\theta_P\right). \end{aligned}$$

Here, $\vec{\boldsymbol{L}}_c$ denotes a vector that connects the origin to a point on the ICP when the direction of movement relative to the wind is θ_G, and $\vec{\boldsymbol{n}}_P$ denotes a unit vector heading to the goal direction. The distance traveled per unit of cost, denoted as $L_C\left(\theta_G, w\right)$, is equal to the distance traveled per unit time (i.e., the ground speed $V(\theta_G, w)$) divided by the amount of cost consumed per unit time (i.e., the cost function $C\left(\theta_G\right)$):

$$L_c\left(\theta_G, w\right) = \frac{V(\theta_G, w)}{C\left(\theta_G\right)}.$$

Thus, the following equation is derived:

$$F(\theta_G|\theta_P, w) = \frac{V(\theta_G, w)}{C(\theta_G)}(\cos\theta_G\cos\theta_P + \sin\theta_G\sin\theta_P).$$

Finally, we assumed that probability distribution of θ_G was proportional to the exponent of $\beta F(\theta_G|\theta_p, w)$, with β as a constant parameter:

$$P(\theta_G|\theta_P, w, \beta) = \frac{e^{\beta F(\theta_G|\theta_P, w)}}{Z(w, \theta_P, \beta)},$$

where $P(\theta_G|\theta_P, w, \beta)$ represents the probability distribution of θ_G given parameters θ_P, w and β. The term $Z(\theta_P, w, \beta)$ represents the normalizing constant such that $\int_{-\pi}^{\pi} P(\theta_G|\theta_P, w, \beta)d\theta_G = 1$, and thus is defined as $Z(\theta_P, w, \beta) = \int_{-\pi}^{\pi} e^{\beta F(\theta_G|\theta_P, w)}d\theta_G$.

From the above, we were able to model the birds' direction of movement through the probability distribution $P(\theta_G|\theta_P, w, \beta)$. This distribution is composed of the functions $V(\theta_G, w)$ and $C(\theta_G)$. The ground speed $V(\theta_G, w)$ is already determined from the experimental data (*Identification of Polar Diagram Using GAM*). Thus, we need to define the specific form of the function $C(\theta_G)$.

[Step 2] formulation of cost functions. The cost function $C(\theta_G)$ should ideally be simple while still capturing the characteristics of the assumed cost. To this end, we have formulated the cost function using polynomials up to the second-order of absolute value of θ_G. We describe the assumed cost for each of the functional forms. These cost functions include some parameters, and we only allow parameters that keep the cost functions positive in the range of $0 \leq |\theta_G| \leq \pi$.

For the constant function, where the cost is time,

$$C(\theta_G) = 1.$$

The consumed cost per time does not change depending on the travel direction. In this case, the travel cost is time.

For the linear function, where the cost is energy,

$$C(\theta_G) = 1 + c_1|\theta_G|.$$

When $c_1 > 0$, the cost function increases when moving upwind, consistent with reports that heart rate, i.e., a good proxy of energy consumption rate, in albatrosses also increases under such conditions (24). This model, therefore, posits that energy constitutes the cost.

For the quadratic function, where the specific cost is unknown,

$$C(\theta_G) = 1 + c_2(|\theta_G| - c_3)^2.$$

We assume that $c_2 > 0$. It reaches its minimum when moving in the direction of c_3, and increases with any deviation from c_3, whether upwind or downwind.

[Step 3] stochastic model and calculation of the likelihood from the data. Our goal was to estimate the cost function that best explains movement data of birds. For this purpose, the likelihood of the model on experimental data should be calculated. We denote the travel direction relative to the wind velocity, wind speed, and goal direction to the wind at time t obtained from individual i as $\Theta_{G,i,t}$, $W_{i,t}$ and $\Theta_{P,i,t}$ $(t = 1, \ldots, T_i)$, respectively. In this case, when the observation data are obtained from n individuals, the likelihood is given by

$$L(\boldsymbol{c}, \beta) = \prod_{i=1}^{n}\prod_{t=1}^{T_i} P(\Theta_{G,i,t}|\Theta_{P,i,t}, W_{i,t}, \boldsymbol{c}, \beta).$$

Where, $\boldsymbol{c} = \{\}$ for constant function, $\boldsymbol{c} = \{c_1\}$ for linear function, and $\boldsymbol{c} = \{c_1, c_2\}$ for quadratic function. For each model that employed the cost functions described above, we computed the parameter $\boldsymbol{c}$ and β that maximize this likelihood, and the BIC. Then, we chose the cost function that best explained the data via model selection based on BIC. The "fminunc" function in MATLAB 2019a was used. The normalization constants $Z(\Theta_{P,i,t}, W_{i,t}, \boldsymbol{c}, \beta)(t = 1, \ldots, T_i, t = 1, \ldots, N)$ were computed numerically by Gaussian quadrature with 360 integration points. The estimated values of BIC and parameters for each model are shown in *SI Appendix*, Tables S2 and S3.

We plotted estimated distributions $P(\theta_G|\theta_P, w, \beta)$ for the BIC-based selected model (pink lines in Fig. 3 *D* and *E*) for $\theta_P = 0, \pm 30°, \pm 60°, \pm 90°, \pm 120°, 120°, \pm 150°, 180°$, and the travel directions that maximize distance traveled in the goal direction per unit of cost spent, corresponding to the peak of this distribution (dashed pink lines in Fig. 3 *D* and *E*). For comparison, VMC maximizing directions were also presented, calculated from the polar diagram identified with GAM (black arrows in Fig. 3 *D* and *E*). These distributions and directions are calculated with wind speed $w = 8.7$ m/s for albatross and 8.9 m/s for sailboats, the average wind speeds they experienced within 500 km from the goal. These two directions across the range of $-180° \leq \theta_P < 180°$ are shown in *SI Appendix*, *SI Appendix01* and Fig. S13.

Data, Materials, and Software Availability. Some study data are available. .csv data of wandering albatrosses have been deposited in GitHub at (64). The standardized data with metadata can be downloaded from the Biologging intelligent Platform (BiP) (https://www.bip-earth.com) (65). DOI of this paper is available to search data used in this paper. The tracking data of sailboats cannot be shared as the ownership belongs to Vendée Globe. Interested readers may contact Vendée Globe for further information (https://www.vendeeglobe.org/en) (66).

ACKNOWLEDGMENTS. We thank Chihiro Kinoshita for illustrating the albatross and sailboats in the figures. We thank Masanobu Katori for providing important information about sailing. We thank Vendée Globe for providing the track data of sailboats. We thank the fieldworkers involved in the study on Crozet, and in particular Julien Collet and Alexandre Corbeau. The field work was supported by Institut Polaire Français Paul-Émile Victor (Program 109, PI H.W.). During the preparation of this work, we used ChatGPT to correct grammar. After interacting with ChatGPT, we meticulously reviewed and made necessary adjustments to the content. We take full responsibility for the content that has been published. This study was financially supported by the Tohoku Ecosystem Associated Marine Science, Grants-in-Aid for Scientific Research from the Japan Society for the Promotion of Science (15J10905, 24241001, 16H06541, 16H01769, 21H05294, 22H00569), National Geographic (Asia 45-16), and Japan Science and Technology Agency, Core Research for Evolutional Science and Technology (JPMJCR1685, JPMJCR23P2, Japan), and by European Research Council (ERC-2012-ADG_20120314 and ERC-2017-PoC_780058).

Author affiliations: [a]Graduate School of Environmental Studies, Nagoya University, Furo, Chikusa, Nagoya 464-8601, Japan; [b]Centre d'Etudes Biologiques Chizé (CEBC), UMR 7372 CNRS–Université de la Rochelle, Villiers En Bois 79360, France; [c]National Institute for Environmental Studies, Tsukuba, Ibaraki 305-8506, Japan; [d]Aeronautical Technology Directorate, Japan Aerospace Exploration Agency (JAXA), Mitaka, Tokyo 181-0015, Japan; and [e]Atmosphere and Ocean Research Institute, The University of Tokyo, Kashiwa, Chiba 277-8564, Japan

1. S. A. Shaffer *et al.*, Migratory shearwaters integrate oceanic resources across the Pacific Ocean in an endless summer. *Proc. Natl. Acad. Sci. U.S.A.* **103**, 12799–12802 (2006).
2. C. Egevang *et al.*, Tracking of Arctic terns Sterna paradisaea reveals longest animal migration. *Proc. Natl. Acad. Sci. U.S.A.* **107**, 2078–2081 (2010).
3. P. Jouventin, H. Weimerskirch, Satellite tracking of wandering albatrosses. *Nature* **343**, 746–748 (1990).
4. H. Weimerskirch, M. Salamolard, F. Sarrazin, P. Jouventin, Foraging strategy of wandering albatrosses through the breeding season: A study using satellite telemetry. *Auk* **110**, 325–342 (1993).
5. R. A. Phillips, J. R. D. Silk, J. P. Croxall, Foraging and provisioning strategies of the light-mantled sooty albatross at South Georgia: Competition and co-existence with sympatric pelagic predators. *Mar. Ecol. Prog. Ser.* **285**, 259–270 (2005).
6. A. Tarroux *et al.*, Flexible flight response to challenging wind conditions in a commuting Antarctic seabird: Do you catch the drift? *Anim. Behav.* **113**, 99–112 (2016).
7. Y. Goto, K. Yoda, K. Sato, Asymmetry hidden in birds' tracks reveals wind, heading, and orientation ability over the ocean. *Sci. Adv.* **3**, e1700097 (2017).
8. F. Ventura, J. P. Granadeiro, O. Padget, P. Catry, Gadfly petrels use knowledge of the windscape, not memorized foraging patches, to optimize foraging trips on ocean-wide scales. *Proc. Biol. Sci.* **287**, 20191775 (2020).
9. J. A. Kempton *et al.*, Optimization of dynamic soaring in a flap-gliding seabird affects its large-scale distribution at sea. *Sci. Adv.* **8**, eabo0200 (2022).
10. T. Alerstam, Wind as selective agent in bird migration. *Ornis Scand.* **10**, 76–93 (1979).
11. J. W. Chapman *et al.*, Animal orientation strategies for movement in flows. *Curr. Biol.* **21**, R861–R870 (2011).
12. T. Alerstam, Optimal use of wind by migrating birds: Combined drift and overcompensation. *J. Theor. Biol.* **79**, 341–353 (1979).
13. W. J. Richardson, Wind and orientation of migrating birds: A review. *EXS* **60**, 226–249 (1991).

14. S. Åkesson, A. Hedenström, How migrants get there: Migratory performance and orientation. *Bioscience* **57**, 123–133 (2007).
15. F. Liechti, A. Hedenström, T. Alerstam, Effects of sidewinds on optimal flight speed of birds. *J. Theor. Biol.* **170**, 219–225 (1994).
16. E. L. C. Shepard *et al.*, Energy landscapes shape animal movement ecology. *Am. Nat.* **182**, 298–312 (2013).
17. Y. Goto, K. Yoda, Developments of theories of avian movement strategies in wind and their validation with bio-logging data. *J. Phys. Soc. Jpn.* **92**, 121006 (2023).
18. K. Sato *et al.*, Scaling of soaring seabirds and implications for flight abilities of giant pterosaurs. *PLoS One* **4**, e5400 (2009).
19. L. Rayleigh, The soaring of birds. *Nature* **27**, 534–535 (1883).
20. G. K. Taylor, K. V. Reynolds, A. L. R. Thomas, Soaring energetics and glide performance in a moving atmosphere. *Philos. Trans. R. Soc. Lond. B Biol. Sci.* **371**, 20150398 (2016).
21. G. D. Bousquet, M. S. Triantafyllou, J.-J. E. Slotine, Optimal dynamic soaring consists of successive shallow arcs. *J. R. Soc. Interface* **14**, 20170496 (2017).
22. G. Sachs, J. Traugott, A. P. Nesterova, F. Bonadonna, Experimental verification of dynamic soaring in albatrosses. *J. Exp. Biol.* **216**, 4222–4232 (2013).
23. Y. Yonehara *et al.*, Flight paths of seabirds soaring over the ocean surface enable measurement of fine-scale wind speed and direction. *Proc. Natl. Acad. Sci. U.S.A.* **113**, 9039–9044 (2016).
24. H. Weimerskirch, T. Guionnet, J. Martin, S. A. Shaffer, D. P. Costa, Fast and fuel efficient? Optimal use of wind by flying albatrosses. *Proc. Biol. Sci.* **267**, 1869–1874 (2000).
25. P. L. Richardson, How do albatrosses fly around the world without flapping their wings? *Prog. Oceanogr.* **88**, 46–58 (2011).
26. P. L. Richardson, E. D. Wakefield, R. A. Phillips, Flight speed and performance of the wandering albatross with respect to wind. *Mov. Ecol.* **6**, 3 (2018).
27. H. Weimerskirch *et al.*, GPS tracking of foraging albatrosses. *Science* **295**, 1259 (2002).
28. H. Weimerskirch, Linking demographic processes and foraging ecology in wandering albatross–Conservation implications. *J. Anim. Ecol.* **87**, 945–955 (2018).
29. E. D. Wakefield *et al.*, Wind field and sex constrain the flight speeds of central-place foraging albatrosses. *Ecol. Monogr.* **79**, 663–679 (2009).
30. F. Ventura *et al.*, A central place foraging seabird flies at right angles to the wind to jointly optimize locomotor and olfactory search efficiency. *Proc. Biol. Sci.* **289**, 20220895 (2022).
31. L. B. Spear, D. G. Ainley, Flight behaviour of seabirds in relation to wind direction and wing morphology. *Ibis* **139**, 221–233 (2008).
32. G. H. Orians, N. E. Pearson, "On the theory of central place foraging" in *Analysis of Ecological Systems*, D. J. Horn, R. Sairs, R. D. Mitchell, Eds. (Ohio State University Press, Columbus, 1979), pp. 155–177.
33. H. Weimerskirch, Are seabirds foraging for unpredictable resources? *Deep Sea Res. Part 2 Top. Stud. Oceanogr.* **54**, 211–223 (2007).
34. G. A. Nevitt, M. Losekoot, H. Weimerskirch, Evidence for olfactory search in wandering albatross, Diomedea exulans. *Proc. Natl. Acad. Sci. U.S.A.* **105**, 4576–4581 (2008).
35. H. Weimerskirch, D. Pinaud, F. Pawlowski, C.-A. Bost, Does prey capture induce area-restricted search? A fine-scale study using GPS in a marine predator, the wandering albatross. *Am. Nat.* **170**, 734–743 (2007).
36. A. Corbeau, J. Collet, M. Fontenille, H. Weimerskirch, How do seabirds modify their search behaviour when encountering fishing boats? *PLoS One* **14**, e0222615 (2019).
37. P. J. Richards, A. Johnson, A. Stanton, America's Cup downwind sails–vertical wings or horizontal parachutes? *J. Wind Eng. Ind. Aerodyn.* **89**, 1565–1577 (2001).
38. D.-N. Liu, Z.-X. Hou, Z. Guo, X.-X. Yang, X.-Z. Gao, Optimal patterns of dynamic soaring with a small unmanned aerial vehicle. *Proc. Inst. Mech. Eng. G J. Aerosp. Eng.* **231**, 1593–1608 (2017).
39. R. Stelzer, T. Pröll, Autonomous sailboat navigation for short course racing. *Rob. Auton. Syst.* **56**, 604–614 (2008).
40. R. M. Johnstone, L. S. Davis, Incubation routines and foraging-trip regulation in the Grey-faced Petrel Pterodroma macroptera gouldi. *Ibis* **132**, 14–20 (1990).
41. H. Weimerskirch, Regulation of foraging trips and incubation routine in male and female wandering albatrosses. *Oecologia* **102**, 37–43 (1995).
42. C. J. Pennycuick, The flight of petrels and albatrosses (procellariiformes), observed in South Georgia and its vicinity. *Philos. Trans. R. Soc. Lond. B Biol. Sci.* **300**, 75–106 (1982).
43. G. Sachs, In-flight measurement of upwind dynamic soaring in albatrosses. *Prog. Oceanogr.* **142**, 47–57 (2016).
44. H. Fritz, S. Said, H. Weimerskirch, Scale-dependent hierarchical adjustments of movement patterns in a long-range foraging seabird. *Proc. Biol. Sci.* **270**, 1143–1148 (2003).
45. G. C. Hays *et al.*, Route optimisation and solving Zermelo's navigation problem during long distance migration in cross flows. *Ecol. Lett.* **17**, 137–143 (2014).
46. N. Horvitz *et al.*, The gliding speed of migrating birds: Slow and safe or fast and risky? *Ecol. Lett.* **17**, 670–679 (2014).
47. R. Harel *et al.*, Decision-making by a soaring bird: Time, energy and risk considerations at different spatio-temporal scales. *Philos. Trans. R. Soc. Lond. B Biol. Sci.* **371**, 20150397 (2016).
48. W. M. G. Vansteelant, J. Shamoun-Baranes, J. McLaren, J. van Diermen, W. Bouten, Soaring across continents: Decision-making of a soaring migrant under changing atmospheric conditions along an entire flyway. *J. Avian Biol.* **48**, 887–896 (2017).
49. C. J. Pennycuick, *Modelling the Flying Bird* (Elsevier, 2008).
50. Z. Akos, M. Nagy, T. Vicsek, Comparing bird and human soaring strategies. *Proc. Natl. Acad. Sci. U.S.A.* **105**, 4139–4143 (2008).
51. G. Sachs, Minimum shear wind strength required for dynamic soaring of albatrosses. *Ibis* **147**, 1–10 (2005).
52. Y. Goto, K. Yoda, H. Weimerskirch, K. Sato, How did extinct giant birds and pterosaurs fly? A comprehensive modeling approach to evaluate soaring performance. *PNAS Nexus* **1**, pgac023 (2022).
53. R. B. Stull, *An Introduction to Boundary Layer Meteorology* (Springer Science & Business Media, 1988).
54. M. P. Buckley, F. Veron, Structure of the airflow above surface waves. *J. Phys. Oceanogr.* **46**, 1377–1397 (2016).
55. A. Bernard, A. S. L. Rodrigues, V. Cazalis, D. Grémillet, Toward a global strategy for seabird tracking. *Conserv. Lett.* **14**, e12804 (2021).
56. E. Lempidakis *et al.*, Pelagic seabirds reduce risk by flying into the eye of the storm. *Proc. Natl. Acad. Sci. U.S.A.* **119**, e2212925119 (2022).
57. E. Nourani *et al.*, Seabird morphology determines operational wind speeds, tolerable maxima, and responses to extremes. *Curr. Biol.* **33**, 1179–1184.e3 (2023).
58. C. Pêtrès, M.-A. Romero-Ramirez, F. Plumet, A potential field approach for reactive navigation of autonomous sailboats. *Rob. Auton. Syst.* **60**, 1520–1527 (2012).
59. H. Saoud, M.-D. Hua, F. Plumet, F. B. Amar, "Routing and course control of an autonomous sailboat" in *2015 European Conference on Mobile Robots* (IEEE, 2015), pp. 1–6.
60. H. Weimerskirch *et al.*, Ocean sentinel albatrosses locate illegal vessels and provide the first estimate of the extent of nondeclared fishing. *Proc. Natl. Acad. Sci. U.S.A.* **117**, 3006–3014 (2020).
61. F. Bonadonna *et al.*, Orientation in the wandering albatross: Interfering with magnetic perception does not affect orientation performance. *Proc. Biol. Sci.* **272**, 489–495 (2005).
62. C. Girard, S. Benhamou, L. Dagorn, FAD: Fish aggregating device or fish attracting device? A new analysis of yellowfin tuna movements around floating objects. *Anim. Behav.* **67**, 319–326 (2004).
63. S. N. Wood, *Generalized Additive Models: An Introduction with R* (Chapman and Hall/CRC, 2006).
64. Y. Goto *et al.*, Data from "Albatrosses employ orientation and routing strategies similar to yacht racers." GitHub. https://github.com/YusukeGoto510/Data_Wandering_Albatross.git. Deposited 22 April 2024.
65. Y. Goto *et al.*, Data from "Albatrosses employ orientation and routing strategies similar to yacht racers." Biologging intelligent Platform (BiP). https://www.bip-earth.com. Deposited 29 April 2024.
66. Vendée Globe, Tracking data of Vendée Globe 2020. Vendée Globe. https://www.vendeeglobe.org/en. Accessed 29 April 2024.